ACS OMEGA

http://pubs.acs.org/journal/acsodf

Article

Selective Cyclized α-Melanocyte-Stimulating Hormone Derivative with Multiple *N*-Methylations for Melanoma Imaging with Positron Emission Tomography

Chengcheng Zhang, Zhengxing Zhang, Jutta Zeisler, Nadine Colpo, Kuo-Shyan Lin, and François Bénard*

Cite This: *ACS Omega* 2020, 5, 10767−10773

Read Online

ACCESS | Metrics & More | Article Recommendations | Supporting Information

ABSTRACT: In this study, we designed and evaluated a novel α-melanocyte-stimulating hormone derivative with four *N*-methylations for melanocortin 1 receptor-targeted melanoma imaging with positron emission tomography (PET). The resulting peptide, DOTA-Pip-Nle^4-Cyclo[Asp^5-*N*-Me-His^6-D-Phe^7-*N*-Me-Arg^8-*N*-Me-Trp^9-*N*-Me-Lys^{10}]αMSH$_{4-10}$-NH$_2$ (CCZ01099), showed high receptor selectivity, greatly improved stability, and rapid internalization. [^{68}Ga]Ga-CCZ01099 showed clear tumor visualization and excellent tumor-to-normal tissue contrast with PET imaging in a preclinical melanoma model. Therefore, CCZ01099 is a promising compound for imaging and potentially radioligand therapy for melanoma.

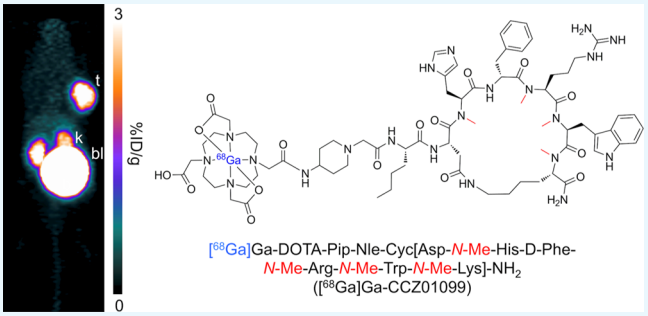

INTRODUCTION

Peptides as diagnostic and therapeutic molecules hold immense potential, thanks to their high target binding affinity, specificity, rapid clearance, low toxicity, and simple chemical synthesis and modifications.[1] The major drawbacks of peptides are usually limited plasma half-life and extremely low oral bioavailability. *N*-Methylation has been recognized to be a robust strategy to modulate biological properties of peptides, including stability, selectivity, and pharmacokinetics.[2,3] The classic example is Cyclosporin A, an undecapeptide with seven *N*-methylations, which has achieved oral bioavailability.[4]

Alpha-melanocyte-stimulating hormone (αMSH), a tridecapeptide, is an endogenous nonselective ligand to the melanocortin (MC) family of receptors. αMSH binds to melanocortin 1 receptor (MC1R) with subnanomolar binding affinity (K_i = 0.23 nM) and also binds to MC3R, MC4R, and MC5R at 31.5, 900, and 7160 nM, respectively.[5] MC2R does not bind to αMSH but interacts with adrenocorticotropic hormone instead. αMSH is synthesized intrinsically by the skin[6] and normal and malignant melanocytes.[7] The expression of αMSH can be upregulated by UV irradiation, particularly UVB.[8,9]

Like most peptides, αMSH has limited stability and is prone to proteolysis *in vivo*. With unnatural amino acid substitutions, truncation, and cyclization, an αMSH derivative called melanotan II (MTII, Ac-Nle^4-Cyclo[Asp^5-His^6-D-Phe^7-Arg^8-Trp^9-Lys^{10}]αMSH$_{4-10}$-NH$_2$) was developed, which showed prolonged biological activity.[10,11] Melanoma imaging targeting MC1R with αMSH derivatives has been extensively studied with the most successful ones based on the MTII sequence (see ref 12 for a recent review). The most popular one is DOTA-GG-Nle-CycMSH$_{hex}$ which is an Nle-CycMSH$_{hex}$ (MTII) derivative conjugated with a DOTA chelator and two additional glycines as the linker. Developed by Miao and colleagues, DOTA-GG-Nle-CycMSH$_{hex}$ showed high tumor uptake in mouse melanoma allografts when complexed with various single photon emission computed tomography (SPECT) isotopes, including ^{111}In,[13] ^{67}Ga,[14] ^{177}Lu (at early time points),[15] and ^{203}Pb.[16] In a recent study, Miao and colleagues employed ^{68}Ga-labeled DOTA-GG-Nle-CycMSH$_{hex}$ and acquired first-in-human positron emission tomography (PET) images of brain metastases in melanoma patients.[17] This demonstrated the clinical relevance of targeting MC1R with MTII for melanoma imaging. However, radionuclide therapy of melanoma using the MTII compound has not seen successful application, one of the key factors is the limited *in vivo* stability of the peptide. This is evident that when DOTA-GG-Nle-CycMSH$_{hex}$ was radiolabeled with ^{177}Lu, a rapid decrease (>60%) in tumor uptake was observed from 2 to 24 h postinjection (p.i.) in a mouse model of melanoma.[15] This suggests that further improvement for the *in vivo* stability of the

Received: January 22, 2020
Accepted: April 28, 2020
Published: May 7, 2020

MTII sequence might be beneficial for the purpose of melanoma treatment.

Moreover, MTII is a nonselective ligand against MC1R, MC3R, MC4R, and MC5R, with average binding affinities at 0.69, 34.1, 6.60, and 46.1 nM, respectively.[5] MC family of receptors are involved in distinct biological functions, including cutaneous and metastatic melanoma (MC1R),[18,19] pigmentation (MC1R),[20] obesity (MC3R and MC4R),[21−23] regulation of metabolism and sexual functions (MC4R),[24] and sebum production (MC5R).[25] Because of the diverse functions of the MC family of receptors, a selective ligand targeting MC1R is desirable.

We recently developed MTII-based imaging probes targeting melanoma with PET and radiolabeled with ^{68}Ga ([^{68}Ga]Ga-CCZ01048)[26] and ^{18}F with ammoniomethyl−trifluoroborate ([^{18}F]CCZ01064).[27] The introduction of a cationic piperidine (Pip) linker motif allowed rapid *in vivo* clearance. In both cases, off-target thyroid uptake was observed. A systematic *N*-methylation scan on the MTII backbone was performed by Hruby and colleagues who identified that *N*-methylations on His^6, Arg^8, Trp^9, and Lys^{10} showed selectivity toward MC1R.[28]

In this study, we aim to synthesize a novel melanoma imaging probe, with four *N*-methylations on MTII, a cationic piperidine linker, and a DOTA chelator, that is, DOTA-Pip-Nle^4-Cyclo[Asp^5-*N*-Me-His^6-D-Phe^7-*N*-Me-Arg^8-*N*-Me-Trp^9-*N*-Me-Lys^{10}]αMSH$_{4-10}$-NH$_2$, namely CCZ01099, and evaluate the effects of *N*-methylations on the MTII backbone in selectivity toward MC1R, *in vivo* stability, and its potential for PET imaging of melanoma.

RESULTS AND DISCUSSION

Peptide synthesis was performed via the standard Fmoc strategy, and the chemical structure of the nonradioactive gallium complexed CCZ01099 (^{nat}Ga-CCZ01099) is shown in Figure 1. *N*-Methylation on the α-amino group of Lys^{10} was performed

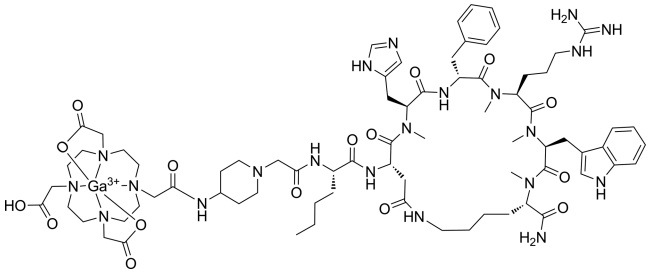

Figure 1. Chemical structure of the multiple *N*-methylated nonradioactive gallium complexed αMSH analogue ^{nat}Ga-CCZ01099.

under Mitsunobu condition, and complete *N*-methylation was observed (Figure S1). *N*-Methylated Fmoc-protected His, Arg, and Trp were used for subsequent couplings to minimize byproducts from incomplete *N*-methylation reactions. The peptide precursor, CCZ01099, was purified by high performance liquid chromatography (HPLC), and its identity was confirmed by mass spectrometry (Figure S2). Nonradioactive gallium complexation of CCZ01099 was performed in acetate buffer. After HPLC purification, ^{nat}Ga-CCZ01099 was obtained with >99% purity (Figure S3), and its identity was confirmed by mass spectrometry (Figure S4). The overall yield of ^{nat}Ga-CCZ01099 was 9%.

To determine the MC1R selectivity of ^{nat}Ga-CCZ01099 as well as the non-*N*-methylated counterpart, ^{nat}Ga-CCZ01048, *in vitro* competitive binding assays were performed using human MC1R, MC3R, MC4R, and MC5R cell membranes with [^{125}I]NDP-αMSH (Figure 2). ^{nat}Ga-CCZ01099 bound to MC1R at nanomolar binding affinity with an average inhibition constant (Ki) of 6.62 nM and showed no specific binding toward MC3R, MC4R, or MC5R. In contrast, without *N*-methylation on the MTII backbone, ^{nat}Ga-CCZ01048 showed specific binding to all four receptors with average Ki values ranging from 0.69 to 83.9 nM. The selectivity result is consistent with the previous study using systematic *N*-methylations on the MTII sequence,[28] indicating that the addition of the DOTA chelator and the piperidine linker did not affect the selectivity of MTII to MC1R. Because of the high binding affinity of ^{nat}Ga-CCZ01048 to MC1R and MC4R, we speculated that the thyroid uptake of [^{68}Ga]Ga-CCZ01048 resulted from MC1R or MC4R expression. However, signals from autoradiography results of mouse thyroid tissue incubated with [^{125}I]NDP-αMSH were not blocked by either MC1R or MC4R selective inhibitor (Figure S5). Nontarget binding may be because of MC3R, MC5R, or other receptors.

CCZ01099 was radiolabeled with ^{68}Ga, the radiochemical yield was 49.4 ± 13.2%, and the molar activity was 105.1 ± 83.17 MBq/nmol (n = 5). The radiochemical purity of [^{68}Ga]Ga-CCZ01099 was >99%, as determined by analytical HPLC (Figure S6). The *in vivo* stability was evaluated in mice at 1 h p.i., and the percentage of intact peptide was ≥98% for [^{68}Ga]Ga-CCZ01099 in mouse urine (Figure 3). In contrast, only 34.0 ± 10.4% of [^{68}Ga]Ga-CCZ01048 remained intact under the same condition. This demonstrated that the *N*-methylations stabilized the peptide backbone of MTII. In addition, internalization assays were performed for both [^{68}Ga]Ga-CCZ01099 and [^{68}Ga]Ga-CCZ01048, 48 and 55% of radioactivity were internalized into the B16−F10 cells at 2 h, respectively (Figure S7). This showed that the *N*-methylations did not alter the internalization property of the MTII derivative. The high *in vivo* stability and internalization characteristics of the *N*-methylated MTII backbone would be particularly beneficial for radiotherapy of cancer when radiolabeled with a therapeutic isotope, for example, ^{177}Lu or ^{225}Ac.

PET imaging and biodistribution studies were performed with [^{68}Ga]Ga-CCZ01099 using C57BL/6J mice bearing B16−F10 melanoma at 1 and 2 h p.i., as well as 1 h p.i. with co-injection of a MC1R-specific inhibitor BMS 470539. B16−F10 tumors were clearly visualized on the PET images, and minimal normal tissue activity was observed except for the kidneys and urinary bladder (Figure 4), indicating that the radioligand was cleared via the renal pathway. Normal tissue activity was further reduced at 2 h p.i. With co-injection of BMS 470539, tumor uptake was abolished, indicating that the tumor uptake of [^{68}Ga]Ga-CCZ01099 was MC1R-mediated. The biodistribution and the tumor-to-normal tissue uptake ratios showed consistent results (Table 1). Tumor and kidney uptake values were 6.33 ± 1.48 and 5.59 ± 0.88% injected dose per gram of tissue (%ID/g) at 1 h p.i., respectively. Minimal normal tissue radioactivity accumulation (<0.8%ID/g) was observed with the majority of the radioactivity cleared through the renal pathway. Blocking with the MC1R-specific inhibitor BMS 470539 resulted in tumor uptake of 0.60 ± 0.15%ID/g (91% reduction, $p < 0.001$). Excellent tumor-to-normal tissue contrast was observed, and the average tumor/muscle, tumor/blood, and tumor/bone uptake ratios were 40.6, 9.94, and 23.3 at 1 h p.i., respectively. These values improved to 125, 27.7, and 52.7 at 2 h p.i., respectively. In addition, the blocking agent drastically reduced the tumor-to-

https://dx.doi.org/10.1021/acsomega.0c00310
ACS Omega 2020, 5, 10767−10773

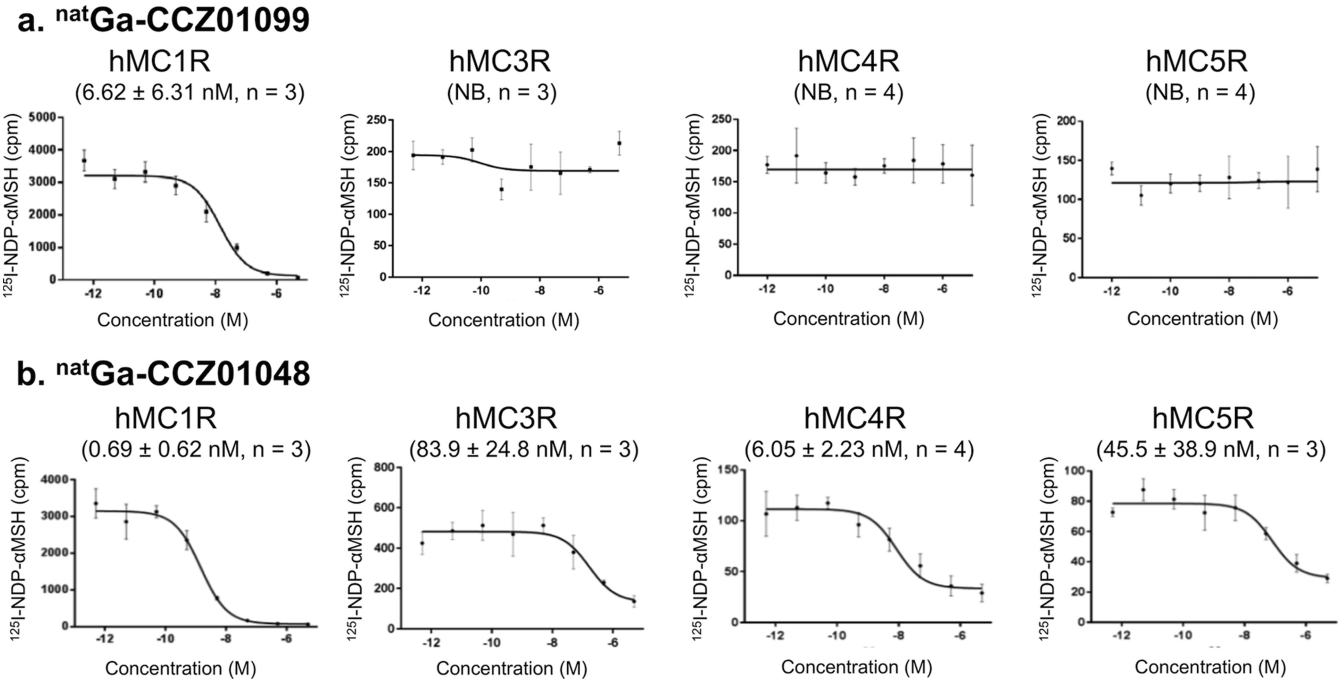

Figure 2. Representative competitive binding curves and inhibition constant (Ki) values of (a) ^{nat}Ga-CCZ01099 and (b) ^{nat}Ga-CCZ01048 to hMC1R, hMC3R, hMC4R, and hMC5R. Three or four independent experiments were performed for each condition, as indicated in the figure. NB, no specific binding observed.

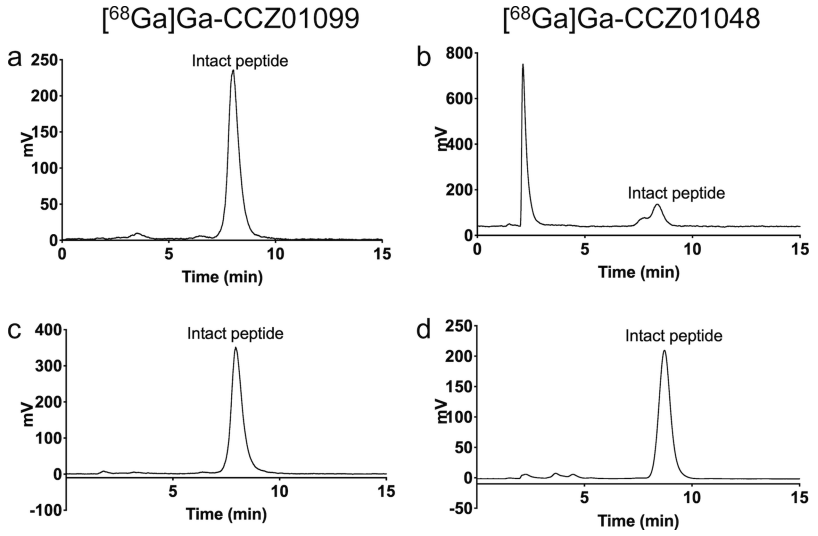

Figure 3. Representative radio-HPLC chromatograms of *in vivo* urine stability of (a) [^{68}Ga]Ga-CCZ01099 ($n = 3$) and (b) [^{68}Ga]Ga-CCZ01048 ($n = 4$) at 1 h p.i. and quality controls for (c) [^{68}Ga]Ga-CCZ01099 and (d) [^{68}Ga]Ga-CCZ01048.

normal tissue contrast as tumor to muscle, blood, bone, and liver uptake ratios decreased by at least 80%. In comparison, with the non-*N*-methylated counterpart, [^{68}Ga]Ga-CCZ01048, a higher tumor uptake value (12.3 ± 3.3%ID/g) was observed at 1 h p.i. in the same tumor model,[26] which is likely because of the higher binding affinity of [^{68}Ga]Ga-CCZ01048 to MC1R. More importantly, off-target thyroid uptake was not observed with [^{68}Ga]Ga-CCZ01099 (0.16 ± 0.03%ID/g), as compared to [^{68}Ga]Ga-CCZ01048 (4.7 ± 1.1%ID/g) at 2 h p.i.[26]

The purpose of this study was to evaluate the effects of *N*-methylations on the MTII backbone and compare the data with those of previously published αMSH derivative, CCZ01048. Therefore, the selection of the DOTA chelator and the piperidine linker remained the same for direct comparison. ^{64}Cu, another PET isotope, has a longer half-life (12.7 h) than ^{68}Ga (68 min), which would allow evaluation of the radiolabeled compounds at longer time points. However, ^{64}Cu-labeled DOTA-GGNle-CycMSH$_{hex}$ showed high normal organ radioactivity accumulation in liver (>10%ID/g), stomach, and lung in a preclinical model of melanoma.[29] These values dropped to the background level when the DOTA chelator was replaced by NOTA,[29] suggesting ^{64}Cu might not be a suitable isotope for the current study with the DOTA-conjugated MTII derivatives. Radiolabeling CCZ01099 with ^{177}Lu (half-life 6.7 days), a SPECT isotope, would be valuable to study biodistribution patterns of the peptide over a few days.

https://dx.doi.org/10.1021/acsomega.0c00310
ACS Omega 2020, 5, 10767−10773

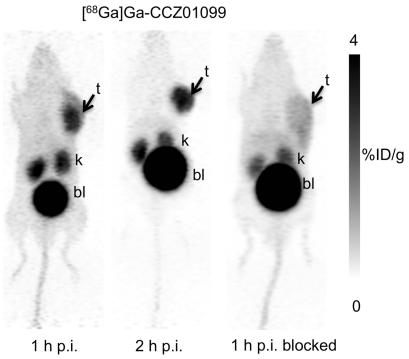

Figure 4. Reconstructed ^{68}Ga-labeled CCZ01099 static PET images (maximum intensity projection) of male C57BL/6J mice bearing B16−F10 tumors at 1 and 2 h p.i., as well as 1 h p.i. blocked with co-injection of 0.5 mg of MC1R-specific inhibitor BMS 470539. Images were taken in duplicate (t, tumor; k, kidney; and bl, bladder).

Table 1. Biodistribution and Tumor-to-Normal Tissue Ratios of ^{68}Ga-Labeled CCZ01099 in Male C57BL/6J Mice Bearing B16−F10 Melanoma at 1 and 2 h p.i. Blocking was Performed by Co-Injection of 0.5 mg of MC1R-Specific Inhibitor BMS 470539 (Two-Way ANOVA Analysis was Performed Comparing 1 h p.i. vs 1 h p.i. Blocked, Multiple Comparisons Were Corrected Using the Holm−Sidak Method, *$p < 0.05$, ***$p < 0.001$)[a]

tissue	1 h p.i. unblocked ($n = 5$)	2 h p.i. unblocked ($n = 4$)	1 h p.i. blocked ($n = 5$)
B16F10 tumor	6.33 ± 1.48	5.22 ± 1.30	0.60 ± 0.15***
blood	0.65 ± 0.12	0.19 ± 0.01	0.27 ± 0.04
fat	0.09 ± 0.04	0.02 ± 0.01	0.04 ± 0.02
seminal glands	0.11 ± 0.06	0.04 ± 0.01	0.07 ± 0.03
testes	0.20 ± 0.06	0.07 ± 0.01	0.10 ± 0.02
intestine	0.34 ± 0.07	0.53 ± 0.38	0.17 ± 0.05
spleen	0.35 ± 0.08	0.19 ± 0.03	0.52 ± 0.28
pancreas	0.17 ± 0.04	0.07 ± 0.01	0.08 ± 0.01
stomach	0.22 ± 0.11	0.20 ± 0.16	0.19 ± 0.12
liver	0.53 ± 0.07	0.44 ± 0.08	0.38 ± 0.11
adrenal glands	0.79 ± 0.72	0.33 ± 0.19	0.45 ± 0.29
kidneys	5.59 ± 0.88	4.42 ± 0.55	2.62 ± 0.91***
heart	0.24 ± 0.06	0.08 ± 0.01	0.13 ± 0.02
lungs	0.69 ± 0.11	0.31 ± 0.05	0.34 ± 0.13
thyroid	0.30 ± 0.08	0.16 ± 0.03	0.13 ± 0.05
bone	0.33 ± 0.18	0.10 ± 0.03	0.17 ± 0.10
muscle	0.16 ± 0.05	0.04 ± 0.00	0.08 ± 0.03
brain	0.05 ± 0.04	0.01 ± 0.00	0.03 ± 0.02
	tumor to normal tissue ratios		
tumor/muscle	40.6 ± 11.9	125 ± 29.6	7.98 ± 1.35***
tumor/blood	9.94 ± 2.93	27.7 ± 5.34	2.24 ± 0.40
tumor/bone	23.3 ± 12.1	52.7 ± 13.4	4.19 ± 1.80***
tumor/liver	11.9 ± 2.26	11.8 ± 2.72	1.79 ± 0.88*
tumor/kidneys	1.13 ± 0.22	1.21 ± 0.44	0.26 ± 0.12

[a]Values are in percentage of injected dose per gram of tissue (%ID/g, mean ± standard deviation).

We selected the B16-F10 mouse melanoma model, which is commonly used for evaluating MC1R-targeted molecular imaging probes because of its high MC1R density (>20,000 copies/cell). This allows the direct comparison of biodistribution and *in vivo* stability between CCZ01099 and CCZ01048 in the same animal model. Care must be taken in interpreting the tumor uptake values because human melanoma cell lines usually have only a few thousand MC1R copies/cell. We recently evaluated [^{68}Ga]Ga-CCZ01048 in a human melanoma xenograft model with the SK-MEL-1 cell line (<1,000 MC1R/cell), which showed tumor uptake of 6.15 ± 0.22%ID/g at 1 h p.i.,[30] as compared to 12.3 ± 3.3%ID/g in the B16F10 mouse melanoma model. The low MC1R density in human melanoma presents a significant challenge in translating the MC1R-targeted imaging probes into the clinic. More investigations need to be carried out to improve the biological half-life of the MTII derivatives, for example, by conjugating an albumin binder to improve tumor uptake.[31]

Nonetheless, the first-in-human pilot study with ^{68}Ga-labeled MTII derivative demonstrated the clinical relevance of targeting MC1R for melanoma imaging.[17] With further optimizations in binding affinity and tumor residence time, *N*-methylated MTII derivatives could be promising backbones for designing radiotherapeutic agents for melanoma treatment.

CONCLUSIONS

In conclusion, we designed and evaluated a MTII peptide derivative with four *N*-methylations, [^{68}Ga]Ga-CCZ01099, which resulted in high MC1R selectivity and *in vivo* stability without affecting the rapid internalization property of the peptide. [^{68}Ga]Ga-CCZ01099 showed MC1R-specific tumor uptake with minimal blood, muscle, and liver radioactivity accumulation in a preclinical model of melanoma using PET imaging. Off-target thyroid uptake was abolished with the introduction of *N*-methylations. The combination of high selectivity, *in vivo* stability, and rapid internalization makes *N*-methylated MTII an important template for developing MC1R-targeted radio-therapeutic agents for melanoma treatment.

EXPERIMENTAL SECTION

Peptide Synthesis of ^{nat}Ga-CCZ01099. CCZ01099, multiple *N*-methylated αMSH analogue DOTA-Pip-Nle-cyclo-[Asp-*N*-Me-His-D-Phe-*N*-Me-Arg-*N*-Me-Trp-*N*-Me-Lys]-αMSH_{4-10}-NH_2, was synthesized via Fmoc chemistry. Fmoc-Rink-Amide-MBHA resin was swelled in dichloromethane, and the Fmoc protecting group was removed by treating the resin with 20% piperidine in *N*,*N*-dimethylformamide. Fmoc-protected amino acid Fmoc-Lys(Mtt)-OH (3 equiv) was coupled to the resin in presence of HATU (3 equiv), HOAt (3 equiv), and DIEA (6 equiv) followed by Fmoc removal. *N*-methylation on the lysine residue was performed under Mitsunobu condition, as previously reported.[28] The free α-amino group was first protected with a 4-nitrobenzenesulfonyl group using a solution of 4-nitrobenzenesulfonyl chloride (Ns-Cl) and 2,4,6-trimethylpyridine (collidine) in 1-methyl-2-pyrrolidone (NMP). *N*-Methylation was achieved in presence of triphenylphosphine, diisopropyl azodicarboxylate, and methanol. Removal of the 4-nitrobenzenesulfonyl protecting group was performed using mercaptoethanol and 1,8-diazabicyclo[5.4.0]undec-7-ene in NMP. Subsequently, Fmoc-protected amino acids, Fmoc-*N*-Me-Trp(Boc)-OH, Fmoc-*N*-Me-Arg(Pbf)-OH, Fmoc-D-Phe-OH, Fmoc-*N*-Me-His(Trt)-OH, Fmoc-Asp(O-2-PhiPr)-OH, and Fmoc-Nle-OH were coupled to the resin sequentially, as described above. Before deprotection of the Fmoc group on the Fmoc-Nle-OH, the Mtt group on the Lys residue and the O-2-PhiPr group on the Asp residue were selectively removed by treatment of 2.5% trifluoroacetic acid. The Lys and the Asp were then cyclized in

https://dx.doi.org/10.1021/acsomega.0c00310
ACS Omega 2020, 5, 10767−10773

presence of HATU (1 equiv), HOAt (1 equiv), and DIEA (2 equiva). The process was repeated until primary amine was no longer detectable by the ninhydrin test. Finally, the Fmoc protecting group was removed, Fmoc-Pip-OH and the DOTA chelator were coupled, as described above.

The peptide was simultaneously deprotected and cleaved from the resin by incubating with 90/5/2.5/2.5 TFA/phenol/H_2O/triisopropylsilane for 1 h at room temperature. The solution containing the peptide was filtered, and the cleaved peptide was precipitated in cold diethyl ether and purified on a semipreparative column using HPLC (Agilent). The HPLC eluate was collected and lyophilized. Mass analysis was performed on a 4000 QTRAP mass spectrometer (AB/Sciex), the calculated mass was 1564.87 $[M + 1H]^+$ and found to be 1564.88 (Figure S2). For gallium complexation, CCZ01099 and $GaCl_3$ (5 equiv) in sodium acetate buffer (0.1 M, pH 4.2) were incubated at 80 °C for 15 min. The mixture was purified by HPLC using a semipreparative column (Phenomenex Luna C18, 5 μm, 250 × 10 mm) eluted with 21% acetonitrile containing 0.1% TFA at a flow rate of 4.5 mL/min. The purity was >99%, as determined by HPLC with an analytical column (Phenomenex Luna C18, 5 μm, 150 × 4.6 mm) using 21% acetonitrile containing 0.1% TFA at a flow rate of 2 mL/min, and the retention time was 7.9 min (Figures S3). The calculated mass for ^{nat}Ga-CCZ01099 was 1630.78 $[M + 1H]^+$ and found to be 1630.76 (Figure S4).

Radiolabeling of [^{68}Ga]Ga-CCZ01099. ^{68}Ga was obtained from a 15/12/A ^{68}Ge/^{68}Ga generator (iThemba Labs) and purified, according to previously published procedures.[32] Briefly, the generator was eluted with 2.5 mL of 0.6 M HCl and mixed with 2 mL of 12 M HCl. The mixture was passed through a DGA resin column, which was subsequently washed by 3 mL of 5 M HCl. After the column was air-dried, ^{68}Ga was eluted off with 0.5 mL of deionized water. The purified ^{68}Ga solution (740−1850 MBq) was mixed with 0.7 mL of HEPES buffer (2 M, pH 5.4) and the DOTA conjugated CCZ01099 or CCZ01048 (25 μg). The radiolabeling reaction was carried out under microwave heating for 1 min. The reaction mixture was purified by HPLC using a semipreparative C18 column eluted with 21% acetonitrile containing 0.1% TFA at a flow rate of 4.5 mL/min. Radiochemical purity of >99% was achieved for the labeled peptides, as determined by radio-HPLC with an analytical column (Phenomenex Luna C18, 5 μm, 150 × 4.6 mm) using 21% acetonitrile containing 0.1% TFA at a flow rate of 2 mL/min, and the retention time was 7.9 min (Figures S6).

MC Receptor Selectivity. *In vitro* competitive binding assays were performed using human MC1R, MC3R, MC4R, and MC5R cell membranes (PerkinElmer), according to the manufacturer's recommended procedures. The membranes were diluted with assay buffer [1:150 dilution, 25 mM HEPES pH 7.0, 1.5 mM $CaCl_2$, 1 mM $MgSO_4$, 100 mM NaCl, 0.2% BSA, 1 mM 1,10-phenanthroline, and 1 complete protease inhibitor tablet (EDTA free)/100 mL], incubated with ^{nat}Ga-CCZ01099/^{nat}Ga-CCZ01048 and [^{125}I][Nle^4, D-Phe^7]-αMSH ([^{125}I]NDP-αMSH, PerkinElmer) at 37 °C with moderate agitation for 1 h. The binding of [^{125}I]NDP-αMSH was completed by the ^{nat}Ga-CCZ01099/^{nat}Ga-CCZ01048 at increasing concentrations from 0.5 pM to 50 μM. After the incubation, the reaction mixture was aspirated, and membranes were washed with ice-cold wash buffer (25 mM HEPES pH 7.0, 1.5 mM $CaCl_2$, 1 mM $MgSO_4$, 100 mM NaCl) via a GC/F filter (presoaked in 0.5% PEI). The radioactivity was measured using a Wallac WIZARD2 gamma counter (PerkinElmer). Three or four independent experiments were performed, for MC1R and MC3R, n = 3 for both ^{nat}Ga-CCZ01099 and ^{nat}Ga-CCZ01048; for MC4R, n = 4 for both ^{nat}Ga-CCZ01099 and ^{nat}Ga-CCZ01048; for MC5R, n = 3 for ^{nat}Ga-CCZ01048, and n = 4 for ^{nat}Ga-CCZ01099.

Animal Studies. All animal experiments were conducted in accordance to the guidelines established by Canadian Council on Animal Care and approved by Animal Ethics Committee of the University of British Columbia. Mice were acquired in-house, housed under pathogen-free conditions, and kept on 12 h light and 12 h dark cycle in the Animal Research Centre, BC Cancer Research Centre, Vancouver, Canada. Male C57BL/6J mice (8−12 weeks of age) were used in this study.

Autoradiography. Autoradiography was performed according to previously published procedures.[33] Briefly, mouse thyroid tissue was harvested and frozen in Tissue plus O.C.T. compound (Fisher Healthcare), and 10 μm sections were obtained using a cryostat (Leica) on Superfrost Plus Gold slides (Fisherbrand). The sections were fixed in methanol for 5 min and prewashed with buffer containing 170 mM Tris−HCl (pH 8.2), 2 mM $CaCl_2$, 5 mM KCl, and 0.5% BSA for 10 min at room temperature. The sections were incubated with 0.1 nM [^{125}I]NDP-αMSH in 170 mM Tris−HCl (pH 8.2), 1% BSA, and 10 mM $MgCl_2$ for 1 h at room temperature without or with 10 μM BMS 470539 (MC1R selective inhibitor, Tocris) or 10 μM MCL 0020 (MC4R selective inhibitor, Tocris). Sections were washed twice with ice-cold buffer containing 170 mM Tris−HCl (pH 8.2) and 0.25% BSA, followed by one time wash with deionized water. The sections were exposed to a phosphor screen and imaged 24 h later using a Typhoon FLA 9500 instrument (GE Healthcare). The experiments were performed in duplicates.

***In Vivo* Stability.** Mice were anesthetized by inhalation with 2% isoflurane in 2.0 L/min of oxygen, and approximately 4−6 MBq of [^{68}Ga]Ga-CCZ01099 or [^{68}Ga]Ga-CCZ01048 was injected intravenously. The mice were allowed to recover and roam freely in their cages. At 1 h p.i., the mice were euthanized by CO_2 inhalation, and their urine was collected and analyzed on HPLC for metabolite using the conditions described above. Three or four independent experiments were performed (n = 3 for [^{68}Ga]Ga-CCZ01099 and n = 4 for [^{68}Ga]Ga-CCZ01048).

Internalization Assay. Internalization assays were carried out using B16−F10 cells seeded onto a 24-well poly-D-lysine plate overnight. ^{68}Ga-labeled peptide was added to the cells, and the mixture was incubated with mild agitation at 37 °C for 30, 60, 90, or 120 min. After removal of the radiolabeled peptide solution, the cells were washed twice with phosphate-buffered saline (PBS). Subsequently, the membrane-bound fraction was collected via acid incubation (0.2 M acetic acid, 0.5 M NaCl, pH 2.6) for 10 min on ice. This step was repeated one more time, and acid solutions were combined. The cells were then washed one more time with PBS and trypsinized to collect the internalized fraction. Both the membrane-bound and internalized fractions were measured for radioactivity using a WIZARD 2480 gamma counter. The total cell-bound activity was the sum of the membrane-bound and internalized counts. The experiments were performed in triplicates or quadruplicates (n = 4 for [^{68}Ga]Ga-CCZ01099 and n = 3 for [^{68}Ga]Ga-CCZ01048).

Cell Culture and Tumor Implantation. B16−F10 melanoma cell line (*Mus musculus*) used in the tumor model was obtained commercially from ATTC (CRL-6475). Cells were cultured in Dulbecco's modified Eagle's medium (Stemcell Technologies) supplemented by 10% fetal bovine serum, 100

https://dx.doi.org/10.1021/acsomega.0c00310
ACS Omega 2020, 5, 10767−10773

U/mL penicillin, and 100 μg/mL streptomycin at 37 °C in a humidified incubator containing 5% CO_2. Cells grown to roughly 90% confluence were washed with sterile PBS (1× PBS, pH 7.4), followed by trypsinization. For tumor implantation, C57BL/6J mice were anesthetized by inhalation with 2% isoflurane, 1 × 10^6 B16−F10 cells were inoculated subcutaneously on right dorsal flank. Mice were imaged or used in biodistribution studies once the tumor reached 6−8 mm in diameter.

PET/CT Imaging and Biodistribution. PET imaging experiments were conducted using a preclinical micro PET/CT scanner (Siemens Inveon). For a static PET scan, each tumor-bearing mouse was injected with 4−6 MBq of ^{68}Ga-labeled CCZ01099 via tail vein under anesthesia. After the injection, mice were allowed to recover and roam freely in their cages. At 1 or 2 h p.i., the mice were sedated again with 2% isoflurane inhalation, positioned in the scanner, and kept warm by a heating pad. A 10 min baseline computed tomography (CT) scan using 60 kV X-rays at 500 μA was obtained for localization and attenuation correction after segmentation for reconstructing the PET images. A single 10−15 min static PET scan was acquired following the CT scan. The mice were euthanized using CO_2 inhalation after imaging. Similar to PET/CT imaging, tumor-bearing mice were injected with 1−2 MBq of ^{68}Ga-labeled CCZ01099 via tail vein under anesthesia with or without co-injection of 0.5 mg of MC1R-specific inhibitor BMS 470,539. At 1 or 2 h p.i., the mice were anesthetized again and euthanized by CO_2 inhalation. Blood was promptly withdrawn, and the organs of interest were harvested, rinsed with 1× PBS (pH 7.4), and blotted dry. Each organ was then weighed, and the radioactivity of the collected tissue was measured using a Wallac WIZARD2 gamma counter, normalized to the injected dose using a standard curve, and expressed as the percentage of the injected dose per gram of tissue (%ID/g).

Statistical Analysis. Statistical analysis was performed using GraphPad Prism 8.1.0. Two-way ANOVA analysis was performed for comparing unblocked and blocked groups in the biodistribution studies. Multiple comparisons were corrected using the Holm−Sidak method. The difference was considered to be statistically significant when p value was <0.05.

■ ASSOCIATED CONTENT

Supporting Information

The Supporting Information is available free of charge at https://pubs.acs.org/doi/10.1021/acsomega.0c00310.

Analytical data, mass spectra, analytical HPLC chromatography, autoradiography, and internalization assay (PDF)

Molecular formula strings (CSV)

The Supporting Information is available free of charge on the ACS Publications website

■ AUTHOR INFORMATION

Corresponding Author

François Bénard − *Department of Molecular Oncology, BC Cancer, Vancouver, British Columbia V5Z 1L3, Canada; Department of Radiology, University of British Columbia, Vancouver, British Columbia V5Z 1M9, Canada;* orcid.org/0000-0001-7995-3581; Phone: 604-675-8206; Email: fbenard@bccrc.ca; Fax: 604-675-8218

Authors

Chengcheng Zhang − *Department of Molecular Oncology, BC Cancer, Vancouver, British Columbia V5Z 1L3, Canada;* orcid.org/0000-0001-5786-4748

Zhengxing Zhang − *Department of Molecular Oncology, BC Cancer, Vancouver, British Columbia V5Z 1L3, Canada*

Jutta Zeisler − *Department of Molecular Oncology, BC Cancer, Vancouver, British Columbia V5Z 1L3, Canada*

Nadine Colpo − *Department of Molecular Oncology, BC Cancer, Vancouver, British Columbia V5Z 1L3, Canada;* orcid.org/0000-0001-9253-6539

Kuo-Shyan Lin − *Department of Molecular Oncology, BC Cancer, Vancouver, British Columbia V5Z 1L3, Canada; Department of Radiology, University of British Columbia, Vancouver, British Columbia V5Z 1M9, Canada;* orcid.org/0000-0002-0739-0780

Complete contact information is available at: https://pubs.acs.org/10.1021/acsomega.0c00310

Funding

This work was supported in part by the Canadian Institutes of Health Research (FDN-148465 and MOP-119361), the BC Cancer Foundation, and the BC Leading Edge Endowment Fund.

Notes

The authors declare no competing financial interest.

■ ACKNOWLEDGMENTS

The authors would like to thank Dr. Jinhe Pan and Guillaume Langlois for their technical assistance.

■ ABBREVIATIONS

PET, positron emission tomography; αMSH, alpha-melanocyte-stimulating hormone; MC1R, melanocortin 1 receptor; MTII, melanotan; p.i., post-injection; DMF, dimethylformamide; DCM, dichloromethane; HATU, 1-[bis(dimethylamino)-methylene]-1H-1,2,3-triazolo[4,5-*b*]pyridinium 3-oxide hexafluorophosphate; HOAt, 1-hydroxy-7-azabenzotriazole; DIEA, *N*,*N*-diisopropylethylamine; DBU, 1,8-diazabicyclo[5.4.0]-undec-7-ene; collidine, 2,4,6-trimethylpyridine; DIAD, diisopropyl azodicarboxylate; TFA, trifluoroacetic acid; HPLC, high performance liquid chromatography

■ REFERENCES

(1) Lau, J. L.; Dunn, M. K. Therapeutic peptides: Historical perspectives, current development trends, and future directions. *Bioorg. Med. Chem.* **2018**, *26*, 2700−2707.

(2) Chatterjee, J.; Rechenmacher, F.; Kessler, H. N-methylation of peptides and proteins: an important element for modulating biological functions. *Angew. Chem., Int. Ed. Engl.* **2013**, *52*, 254−269.

(3) Räder, A. F. B.; Reichart, F.; Weinmüller, M.; Kessler, H. Improving oral bioavailability of cyclic peptides by N-methylation. *Bioorg. Med. Chem.* **2018**, *26*, 2766−2773.

(4) Smith, J. M.; Hows, J. M.; Gordon-Smith, E. C. Stability of cyclosporin A in human serum. *J. Clin. Pathol.* **1983**, *36*, 41−43.

(5) Schiöth, H. B.; Muceniece, R.; Mutulis, F.; Prusis, P.; Lindeberg, G.; Sharma, S. D.; Hruby, V. J.; Wikberg, J. E. S. Selectivity of cyclic [D-Nal7] and [D-Phe7] substituted MSH analogues for the melanocortin receptor subtypes. *Peptides* **1997**, *18*, 1009−1013.

(6) Slominski, A.; Wortsman, J.; Luger, T.; Paus, R.; Solomon, S. Corticotropin releasing hormone and proopiomelanocortin involvement in the cutaneous response to stress. *Physiol. Rev.* **2000**, *80*, 979−1020.

(7) Slominski, A.; Tobin, D. J.; Shibahara, S.; Wortsman, J. Melanin pigmentation in mammalian skin and its hormonal regulation. *Physiol. Rev.* **2004**, *84*, 1155−1228.
(8) Slominski, A. T.; Zmijewski, M. A.; Plonka, P. M.; Szaflarski, J. P.; Paus, R. How UV light touches the brain and endocrine system through skin, and why. *Endocrinology* **2018**, *159*, 1992−2007.
(9) Slominski, A. T.; Zmijewski, M. A.; Zbytek, B.; Tobin, D. J.; Theoharides, T. C.; Rivier, J. Key role of CRF in the skin stress response system. *Endocr. Rev.* **2013**, *34*, 827−884.
(10) Hadley, M. E.; Marwan, M. M.; al-Obeidi, F.; Hruby, V. J. Linear and Cyclic α-Melanotropin [4−10]-Fragment Analogues That Exhibit Superpotency and Residual Activity. *Pigm. Cell Res.* **1989**, *2*, 478−484.
(11) Lauro Castrucci, F.; Castrucci, A. M. d. L.; Hadley, M. E.; Hruby, V. J. Potent and prolonged-acting cyclic lactam analogs of. alpha.-melanotropin: design based on molecular dynamics. *J. Med. Chem.* **1989**, *32*, 2555−2561.
(12) Zhang, C.; Lin, K.-S.; Bénard, F. Molecular Imaging and Radionuclide Therapy of Melanoma Targeting the Melanocortin 1 Receptor. *Mol. Imag.* **2017**, *16*, 153601211773791.
(13) Guo, H.; Yang, J.; Gallazzi, F.; Miao, Y. Effects of the Amino Acid Linkers on the Melanoma-Targeting and Pharmacokinetic Properties of 111In-Labeled Lactam Bridge−Cyclized α-MSH Peptides. *J. Nucl. Med.* **2011**, *52*, 608−616.
(14) Guo, H.; Gallazzi, F.; Miao, Y. Gallium-67-labeled lactam bridge-cyclized alpha-MSH peptides with enhanced melanoma uptake and reduced renal uptake. *Bioconjugate Chem.* **2012**, *23*, 1341−1348.
(15) Guo, H.; Miao, Y. Melanoma targeting property of a Lu-177-labeled lactam bridge-cyclized alpha-MSH peptide. *Bioorg. Med. Chem. Lett.* **2013**, *23*, 2319−2323.
(16) Yang, J.; Xu, J.; Cheuy, L.; Gonzalez, R.; Fisher, D. R.; Miao, Y. Evaluation of a Novel Pb-203-Labeled Lactam-Cyclized Alpha-Melanocyte-Stimulating Hormone Peptide for Melanoma Targeting. *Mol. Pharm.* **2019**, *16*, 1694−1702.
(17) Yang, J.; Xu, J.; Gonzalez, R.; Lindner, T.; Kratochwil, C.; Miao, Y. 68Ga-DOTA-GGNle-CycMSHhex targets the melanocortin-1 receptor for melanoma imaging. *Sci. Transl. Med.* **2018**, *10*, No. eaau4445.
(18) Salazar-Onfray, F.; López, M.; Lundqvist, A.; Aguirre, A.; Escobar, A.; Serrano, A.; Korenblit, C.; Petersson, M.; Chhajlani, V.; Larsson, O.; Kiessling, R. Tissue distribution and differential expression of melanocortin 1 receptor, a malignant melanoma marker. *Br. J. Cancer* **2002**, *87*, 414−422.
(19) López, M. N.; Pereda, C.; Ramirez, M.; Mendoza-Naranjo, A.; Serrano, A.; Ferreira, A.; Poblete, R.; Kalergis, A. M.; Kiessling, R.; Salazar-Onfray, F. Melanocortin 1 receptor is expressed by uveal malignant melanoma and can be considered a new target for diagnosis and immunotherapy. *Invest. Ophthalmol. Vis. Sci.* **2007**, *48*, 1219−1227.
(20) Kadekaro, A. L.; Kanto, H.; Kavanagh, R.; Abdel-malek, Z. A. Significance of the melanocortin 1 receptor in regulating human melanocyte pigmentation, proliferation, and survival. *Ann. N. Y. Acad. Sci* **2003**, *994*, 359−365.
(21) Lee, Y.-S.; Poh, L. K.-S.; Loke, K.-Y. A novel melanocortin 3 receptor gene (MC3R) mutation associated with severe obesity. *J. Clin. Endocrinol. Metab.* **2002**, *87*, 1423−1426.
(22) Huszar, D.; Lynch, C. A.; Fairchild-Huntress, V.; Dunmore, J. H.; Fang, Q.; Berkemeier, L. R.; Gu, W.; Kesterson, R. A.; Boston, B. A.; Cone, R. D.; Smith, F. J.; Campfield, L. A.; Burn, P.; Lee, F. Targeted disruption of the melanocortin-4 receptor results in obesity in mice. *Cell* **1997**, *88*, 131−141.
(23) Farooqi, I. S.; Keogh, J. M.; Yeo, G. S. H.; Lank, E. J.; Cheetham, T.; O'Rahilly, S. Clinical spectrum of obesity and mutations in the melanocortin 4 receptor gene. *N. Engl. J. Med.* **2003**, *348*, 1085−1095.
(24) Van der Ploeg, L. H. T.; Martin, W. J.; Howard, A. D.; Nargund, R. P.; Austin, C. P.; Guan, X.; Drisko, J.; Cashen, D.; Sebhat, I.; Patchett, A. A.; Figueroa, D. J.; DiLella, A. G.; Connolly, B. M.; Weinberg, D. H.; Tan, C. P.; Palyha, O. C.; Pong, S.-S.; MacNeil, T.; Rosenblum, C.; Vongs, A.; Tang, R.; Yu, H.; Sailer, A. W.; Fong, T. M.; Huang, C.; Tota, M. R.; Chang, R. S.; Stearns, R.; Tamvakopoulos, C.; Christ, G.; Drazen, D. L.; Spar, B. D.; Nelson, R. J.; MacIntyre, D. E. A role for the melanocortin 4 receptor in sexual function. *Proc. Natl. Acad. Sci. U. S. A.* **2002**, *99*, 11381−11386.
(25) Van Der Kraan, M.; Adan, R. A. H.; Entwistle, M. L.; Gispen, W. H.; Burbach, J. P. H.; Tatro, J. B. Expression of melanocortin-5 receptor in secretory epithelia supports a functional role in exocrine and endocrine glands. *Endocrinology* **1998**, *139*, 2348−2355.
(26) Zhang, C.; Zhang, Z.; Lin, K.-S.; Pan, J.; Dude, I.; Hundal-Jabal, N.; Colpo, N.; Bénard, F. Preclinical Melanoma Imaging with 68Ga-Labeled α-Melanocyte-Stimulating Hormone Derivatives Using PET. *Theranostics* **2017**, *7*, 805−813.
(27) Zhang, C.; Zhang, Z.; Lin, K.; Lau, J.; Zeisler, J.; Colpo, N.; Perrin, D.; Benard, F. Melanoma imaging using 18F-labeled α-melanocyte-stimulating hormone derivatives with positron emission tomography. *Mol Pharm* **2018**, *15*, 2116.
(28) Doedens, L.; Opperer, F.; Cai, M.; Beck, J. G.; Dedek, M.; Palmer, E.; Hruby, V. J.; Kessler, H. Multiple N-methylation of MT-II backbone amide bonds leads to melanocortin receptor subtype hMC1R selectivity: pharmacological and conformational studies. *J. Am. Chem. Soc.* **2010**, *132*, 8115−8128.
(29) Guo, H.; Miao, Y. Cu-64-labeled lactam bridge-cyclized α-MSH peptides for PET imaging of melanoma. *Mol. Pharm.* **2012**, *9*, 2322−2330.
(30) Zhang, C.; Zhang, Z.; Merkens, H.; Zeisler, J.; Colpo, N.; Hundal-Jabal, N.; Perrin, D. M.; Lin, K.-S.; Bénard, F. 18 F-Labeled Cyclized α-Melanocyte-Stimulating Hormone Derivatives for Imaging Human Melanoma Xenograft with Positron Emission Tomography. *Sci. Rep.* **2019**, *9*, 1−10.
(31) Zhang, C.; Zhang, Z.; Lau, J.; Zeisler, J.; Colpo, N.; Lin, K.-S.; Benard, F. Targeting the melanocortin-1 receptor with 177Lu-labeled alpha-melanocyte stimulating hormone derivatives: increased tumor uptake using an albumin binder. *J. Nucl. Med.* **2018**, *59*, 1106.
(32) Lin, K.-S.; Pan, J.; Amouroux, G.; Turashvili, G.; Mesak, F.; Hundal-Jabal, N.; Pourghiasian, M.; Lau, J.; Jenni, S.; Aparicio, S.; Bénard, F. In vivo radioimaging of bradykinin receptor B1, a widely overexpressed molecule in human cancer. *Cancer Res.* **2015**, *75*, 387−393.
(33) Zhang, C.; Pan, J.; Lin, K.-S.; Dude, I.; Lau, J.; Zeisler, J.; Merkens, H.; Jenni, S.; Guérin, B.; Bénard, F. Targeting the neuropeptide Y1 receptor for cancer imaging by positron emission tomography using novel truncated peptides. *Mol. Pharm.* **2016**, *13*, 3657−3664.

https://dx.doi.org/10.1021/acsomega.0c00310
ACS Omega 2020, 5, 10767−10773